Laser-machined two-stage nozzle optimised for laser wakefield acceleration

V. Tomkus [1],†, **M. Mackevičiūtė** [1], **J. Dudutis** [1], **V. Girdauskas** [1,2],
M. Abedi-Varaki [1], **P. Gečys** [1] **and G. Račiukaitis** [1]

[1]FTMC - Center for Physical Sciences and Technology, Savanoriu Ave. 231, LT-02300 Vilnius, Lithuania

[2]Vytautas Magnus University, K. Donelaicio St. 58, LT-44248 Kaunas, Lithuania

In this paper, the modelling and manufacturing of a two-stage supersonic gas jet nozzle enabling the formation of adaptive plasma concentration profiles for injection and acceleration of electrons using few-cycle laser beams are presented. The stages are modelled using the rhoSimpleFoam algorithm of the OpenFOAM computational fluid dynamics software. The first 200–300 µm diameter nozzle stage is dedicated to 1 % N_2 + He gas jet formation and electron injection. By varying the pressure between the first and second stages of the injectors, the electron injection location could be adjusted, and the maximum acceleration distance could be ensured. By changing the concentration of the nitrogen in the gas mixture, the charge of the accelerated electrons could be controlled. The second nozzle stage is designed for acceleration in fully ionised He or hydrogen gas and forms the optimal plasma concentration for bubble formation depending on the laser pulse energy, duration and focused beam diameter. In order to reduce the diameter of the plasma profile formed by the first nozzle and the concentration drop gap between the two nozzles, a one-side straight section was introduced in the first nozzle. The shock wave reflected from the straight section of the wall propagates parallel to the shock wave of the intersecting supersonic jets and ensures a minimal gap between the jets. The second-stage longitudinal plasma concentration profile could have an increasing gas density gradient to compensate for dephasing between the electron bunch and the plasma wave due to wave shortening with increasing plasma concentration.

Keywords: laser wakefield acceleration, electron acceleration, two-stage gas nozzle, plasma applications, plasma devices

1. Introduction

In laser wakefield acceleration (LWFA), the ponderomotive force of the intense laser pulse drives plasma electrons outward, forming plasma waves that travel at relativistic speeds along with the laser pulse. The electrons trapped in the plasma wave can be accelerated up to GeV energies in an efficient and compact way (Tajima & Malka

† Email address for correspondence: vidmantas.tomkus@ftmc.lt

2020). Numerical and experimental studies have been conducted on a wide variety of injection methods to produce quasi-monoenergetic electron beams, such as self-injection (Kalmykov *et al.* 2009; Mangles *et al.* 2012; Wan *et al.* 2022), ionisation injection (McGuffey *et al.* 2010; Pak *et al.* 2010) and density down-ramp injection (Schmid *et al.* 2010; Buck *et al.* 2013; Foerster *et al.* 2022). The electron injection based on a down-ramp plasma density transition profile has proved to be an effective technique for high-quality LWFA electron beam acceleration (Schmid *et al.* 2010; Buck *et al.* 2013; Wang *et al.* 2021). A lot of research has been done on density down-ramp injection in beam-driven plasma wakefield acceleration (Suk *et al.* 2001; De La Ossa *et al.* 2017; Xu *et al.* 2017). This technique has been employed recently for free-electron lasing using a high-quality LWFA electron beam of 10–50 pc (Schmid *et al.* 2010; Buck *et al.* 2013; Wang *et al.* 2021). Ionisation injection schemes with nitrogen-mixed light gases such as He or H2 and pure He or H2 in a second section were investigated by Golovin *et al.* (2016). Nevertheless, due to the nonlinear laser propagation in LWFA plasma, it is challenging to analyse the injection mechanisms (Vieira *et al.* 2010).

One of the most essential features of LWFA is the capability to create a suitable gas density profile for the controlled injection of electrons into the accelerator phase while maintaining the optimal plasma concentration for acceleration. One common method of creating desired density profiles is by producing a supersonic gas nozzle. The demand for stable, energetic e-beams with a wide energy range, low energy spread and high charge is prevalent in a variety of applications. Due to the differences in injection and acceleration requirements, those characteristics have been difficult to achieve simultaneously in single-stage LWFA. In electron acceleration, for instance, low-density plasma is needed since it has longer dephasing ($L_{deph} \propto n^{-3/2}$) and depletion lengths ($L_{depl} \propto n^{-1}$). However, self-trapping in low-density plasma is ineffective at injecting charge and provides little control over generated electron beams. To overcome this issue, several approaches have been introduced. Instead of self-trapping, these methods deterministically force background plasma electrons to become locally dephased and then become trapped and eventually accelerated by the plasma wave. There are several experimental studies (Gonsalves *et al.* 2011; Liu *et al.* 2011; Pollock *et al.* 2011; Kim *et al.* 2013; Wang *et al.* 2013; Vargas *et al.* 2014; Golovin *et al.* 2016; Steinke *et al.* 2016) that physically separate the injector and accelerator stages, but in most cases, these supersonic nozzles or gas cells were designed for LWFA using multi-terawatt joule class lasers with pulse duration of 30 fs. The lower plasma concentration and relatively long pulse duration result in a millimetre-scale acceleration distance. Such gas targets are manufactured using regular computer numerical control or additive printing technology. In the case of kilohertz lasers with few-cycle pulse duration and limited energy, the acceleration distance shrinks to a few hundred microns, and tailoring of plasma targets becomes challenging. Stable LWFA acceleration using a near one-cycle laser and a one-side-shock nozzle manufactured using hybrid fused silica machining technology was demonstrated in Rovige *et al.* (2020). An alternative design of an LWFA target is presented in this paper, which consists of two-stage gas micrometric nozzles: the injector, which uses mixed gas (helium with a small percentage of nitrogen), and the accelerator (with pure helium). This approach offers the advantage of independent control of the plasma concentration of the injection and acceleration stage. A novel focusing tool – an axiparabola proposed for broadband high-intensity lasers – produces Bessel–Gauss beams and allows for tuning of the phase of the plasma wave (Smartsev *et al.* 2019; Oubrerie *et al.* 2022). Therefore, a short injector zone with a longer acceleration distance could be required relative to the gas target formed by a circular supersonic nozzle. Several scholars have also investigated density injection

parameters numerically (Samant, Upadhyay, & Krishnagopal 2014; Ekerfelt *et al.* 2017; Massimo *et al.* 2017).

Nowadays, emerging kilohertz laser systems, generating few-cycle laser pulses with tens of mJ of energy, provide peak intensities in the range of 10^{18}–10^{19} W cm^{-2} and can be efficiently used for particle acceleration (He 2014; Zhang *et al.* 2022; Tóth *et al.* 2023). To drive the charged particles in the LWFA self-guiding bubble regime, relatively high plasma concentrations of $n = 3$–5×10^{19} cm^{-3} and tighter focusing of the laser beam to the diameter of 3–5 μm are required. This leads to shorter acceleration distances of tens to hundreds of micrometres, resulting in a relatively low energy of the accelerated electrons and high energy spread.

This study aims to simulate and manufacture a two-stage nozzle from a single block of fused silica for injection and LWFA of electrons using few-cycle laser pulses of the Bessel–Gauss beam. The extended focal line of the Bessel–Gauss beam ensures a low diffraction and longer acceleration distance. A one-sided shock nozzle was manufactured using three-dimensional laser machining of fused silica blocks, enabling injection control with a precision of 20–40 μm (Rovige *et al.* 2020). The longitudinal plasma concentration profile of the second stage can include the rising gas density gradient to reach the rephasing thanks to the shifting of the centre of the plasma bubble with a decrease of the plasma wavelength (Sprangle *et al.* 2001; Pukhov & Kostyukov 2008; Guillaume *et al.* 2015; Oubrerie *et al.* 2022).

Different machining techniques are applied for manufacturing converging–diverging channels. Conventional mechanical drilling enables fabrication of channels with diameters usually down to 1 mm (Cai *et al.* 2015, 2016; Cai, Liu, & Shi 2017). However, the converging and diverging parts are manufactured in separate steps (Cai *et al.* 2015, 2017). Although additive manufacturing processes like stereolithography and selective laser sintering are also limited to throat diameters down to 1 mm, complex channels are manufactured in a single step (Döpp *et al.* 2016; Andrianaki *et al.* 2023). Femtosecond laser-induced chemical etching (FLICE), laser trepanning and electrical discharge machining (EDM) can be used to produce diameters smaller than 100 μm (Takahashi *et al.* 2013; Tomkus *et al.* 2019; Chiomento *et al.* 2021; Zuffi *et al.* 2022). However, de Laval-shaped channel formation is typically a two-step process for laser trepanning and EDM techniques (Li *et al.* 2018; Chiomento *et al.* 2021; Zuffi *et al.* 2022). The FLICE technique is more flexible as converging–diverging channels can be formed from one side, and additional alignment and coupling steps can be avoided (Rovige *et al.* 2021). However, FLICE, laser trepanning or EDM of micrometre-scale diameters are limited to low millimetre-scale depths (Takahashi *et al.* 2013; Tomkus *et al.* 2019; Chiomento *et al.* 2021). For larger nozzles, nanosecond rear-side milling is an appealing approach, as centimetre-sized nozzles can be formed with channel diameters down to 100 μm (Tomkus *et al.* 2018; Chaulagain *et al.* 2021). Additionally, this technique can form converging–diverging channels up to some angle in a single step (Chaulagain *et al.* 2021). In this paper, we demonstrate fabrication of a two-stage nozzle from a single block of fused silica using the rear-side milling technique only.

2. Numerical modelling of gas propagation

In this article, we propose implementing a two-stage supersonic nozzle to optimise the injection and acceleration of electrons using a Bessel–Gauss driving beam. The two-stage nozzle was simulated using the OpenFOAM computational fluid dynamics (CFD) software (figures 1 and 2) (Chen *et al.* 2014; OpenFOAM, 2022). The first stage of the nozzle with a diameter of 200–300 μm is used for the formation of a 1 % N$_2$ + He gas jet and ionisation injection of electrons. The balance of the backing pressure between
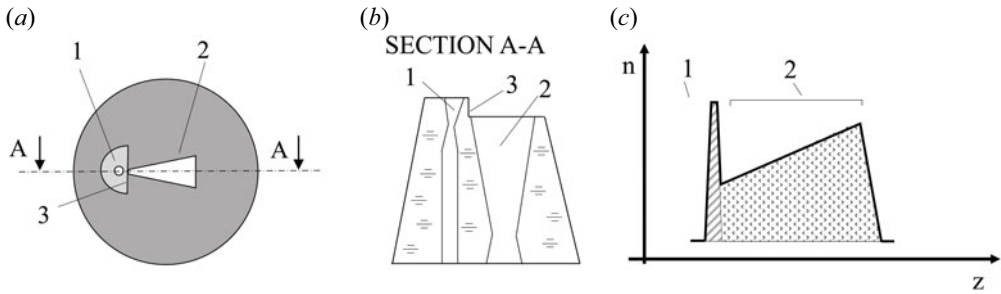
FIGURE 1. Schematic of a two-stage nozzle (*a,b*), consisting of a first electron injection stage (1), a second acceleration stage (2) and a one-half straight wall section (3) that reduces the gas concentration drop between the two nozzles. Longitudinal profile of gas concentration (*c*) to form an increasing gas density gradient.
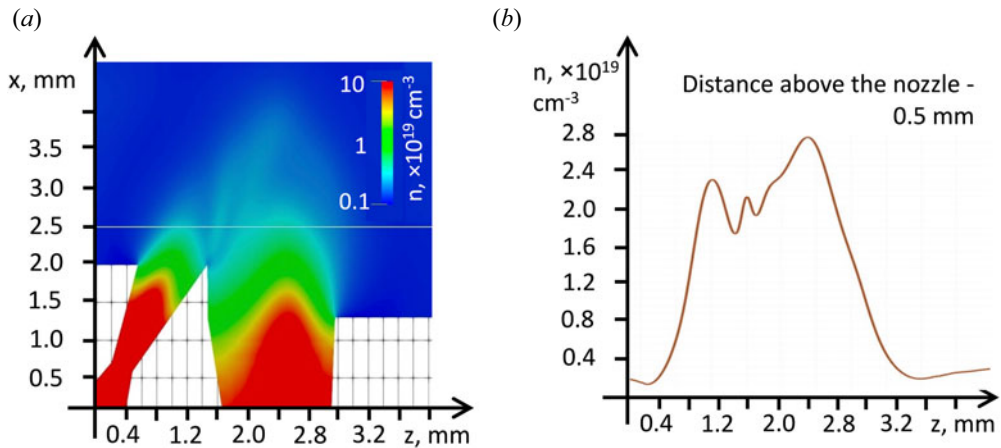

FIGURE 2. Helium gas density diagram of the two-stage supersonic nozzle (*a*) and longitudinal gas concentration profile at the backing pressure of 27 bar along the laser propagation path at a 0.5 mm distance above the outlet of the injection stage of the nozzle (*b*) simulated using the OpenFOAM CFD software.

the first and second nozzle stages allows the injection of electrons into the rear part of the plasma bubble and ensures the maximal acceleration distance. The second stage of the nozzle is dedicated to the LWFA acceleration of electrons in the pure He gas and defines the optimal plasma concentration for the formation of the bubble depending on the pulse energy, duration and diameter of the focused beam. To minimise the gap of the concentration drop between the two jets, a one-side straight section (Rovige *et al.* 2020) was implemented to cause a shock wave reflected from the wall to be colinear to the shock wave from the intersecting supersonic jets. The longitudinal plasma concentration profile of the second stage includes the rising gas density gradient to reach the rephasing and extend the LWFA acceleration distance. It should be noted that helium gas at room temperature 293 K was used in simulations, and the backing pressure was changed from 10 to 50 bar. The corresponding maximal atomic gas concentration at the 500 µm maximum from the nozzle outlet was correspondingly between 1.0×10^{19} and 5.2×10^{19} cm^{-3}. Also, the gas concentration in figures 1 and 2 corresponds to the backing pressure of 27 bar.

3. Methods of laser processing and characterisation

Nozzles with converging–diverging channels have already been manufactured from fused silica using nanosecond laser rear-side milling (Chaulagain *et al.* 2021). However, the most complicated parts of this design are the diverging part of the acceleration channel and the inclined injection channel with an angle of 30°. In this geometry, there is unaffected material below at least part of the scanning contour, increasing the chance of the channel clogging with processing debris. Therefore, it is essential to remove ablated particles from the interaction zone. For this, pulses of high air pressure were blown toward the channel after each layer.

In this study, the nozzle was fabricated with a 532 nm wavelength and 4.5 ns (FWHM) pulse duration (Atlantic 60, Ekspla) three-dimensional laser system using a nanosecond bottom-up machining method (Gečys, Dudutis, & Račiukaitis 2015; Tomkus *et al.* 2018, 2020). The laser beam in the *X* and *Y* axes was controlled by a galvanometric scanner (excelliSCAN 14, Scanlab), and the positioning in the *Z* axis was performed by a motorised translation table (8MT167-100, Standa). The beam was focused using an 80 mm focal length telecentric f-theta lens. The beam waist diameter of 10.8 µm was measured by the Liu's method on a chrome-coated glass sample. Machining was performed on a $100 \times 100 \times 8.2 \, \text{mm}^3$ fused silica block. Initially, the laser beam was focused below the rear side of the sample ((figure 3*a*). The laser beam was scanned in spiral, contour or hatch trajectories (figure 3*b*). After scanning one layer, the sample was lowered by a specific value of *dz* (figure 3*a*). In each subsequent layer, the scan path of the beam was rotated relative to it by an angle of 33°. This was done to achieve a more homogeneous machining regime. Beam scanning and shifting of a sample in the *Z* direction were repeated until the object was cut entirely. It should be noted that the channels were milled by blowing an air current towards them. Air was blown through a 3 mm outlet diameter nozzle, 8.4 mm below the rear side of the sample. After each layer, the air was blown for 100 ms with a pressure of 0.1 MPa. The processing products were removed from the ablation zone with the help of an extraction system (AD Oracle iQ, Bofa International Ltd).

Nozzle milling was divided into 5 stages (figure 3*c*). In the first step, the conical part of the nozzle (step 1) was formed by the spiral scanning algorithm. The spiral algorithm is the fastest because jumps between scan lines could be avoided. The inclined channel for injection was then formed by the spiral scanning algorithm (step 2). Next, the plane part of the nozzle was milled by the hatching algorithm (step 3). The hatching is advantageous for ablating uniform surfaces throughout the processing area. For other algorithms, the thermal accumulation effects are higher for the centre area than for the outer parts. The larger channel for acceleration was milled with a contour algorithm (step 4). It was desired to mill the channels with a scanning algorithm, with which the scanning would be started from the centre to the outside. Since both channels had some parts where the following layers had larger milling areas than the layer before, outward scanning ensured that the ablated particles had a chance to be removed from the milled area. Scanning to the outside can be done with both a spiral and a contour algorithm. The spiral algorithm is optimal for parts with circular shapes. However, the contour scan algorithm was chosen to produce the acceleration channel due to the more complex shape. Finally, the nozzle body was cut entirely out using a spiral algorithm (step 5).

The quality of the milled nozzles was evaluated using an optical microscope (Eclipse LV100NDA, Nikon) and an optical profilometer (S Neox, Sensofar). The roughness of the linear profiles was measured according to ISO 4288:1996.
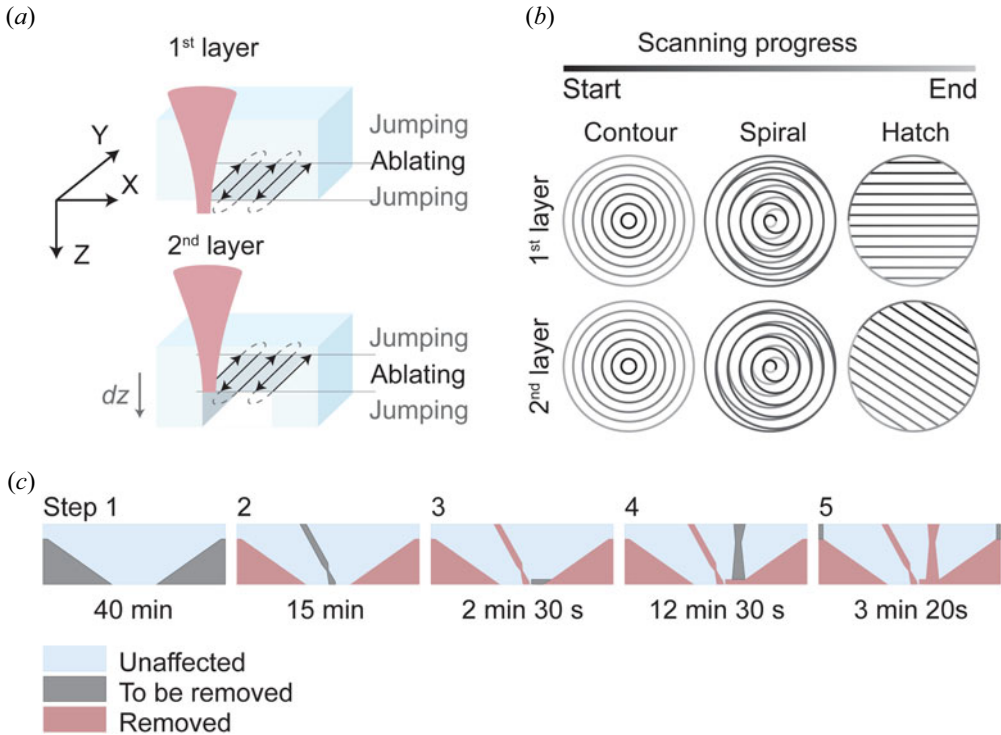
(*a*)

(*b*)

(*c*)

FIGURE 3. (*a*) The scheme of milling and laser scanning; (*b*) contour, spiral and hatch laser scanning algorithms. The darkest colour represents the beginning of the scan, and the brightest colour represents the end. (*c*) The steps of nozzle milling. The grey colour represents the areas to be removed in the corresponding stage, blue – the material not affected by the laser, and red – the already processed part.

4. Nozzle fabrication

The nozzle was milled using 65 μJ pulse energy and a 20 μm distance between the centres of successive irradiated spots along the scanning trajectory. The distance between the sequent scanning lines was 25 μm for the nozzle body and 20 μm for the channels. The nozzle body was milled with a pulse repetition rate of 200 kHz (step 1). This allowed us to reach a high milling rate of 0.75 mm^3 s^{-1} and a milling efficiency of 0.06 mm^3 J^{-1}. Other parts were milled with a lower pulse repetition rate to minimise the thermal accumulation effects. The inclined injection channel (step 2) was milled with a relatively low 1 kHz pulse repetition rate. The plane part (step 3) and acceleration channel (step 4) were milled with repetition rates of 10 kHz and 2 kHz, respectively. The processing time of grey parts in each step is indicated in images above in figure 3*c*. The total milling time was 1 hour and 13 minutes.

A photo of the milled nozzle is shown in figure 4(*a*), and the optical microscope image of the top surface of the nozzle is shown in figure 4(*b*). The top and bottom sides of the injection channel are shown in figures 4(*c*) and 4(*d*), and the top, waist and bottom of the acceleration channel are seen in figures 4(*e*)–4(*g*). The edge chipping at the bottom and top side of the injection nozzle was up to 130 μm and 60 μm, respectively. The chipping of the acceleration nozzle was smaller – up to 120 μm on the bottom side and up to 30 μm on the top side. Both channels had larger chipping on the bottom surface. The reason for
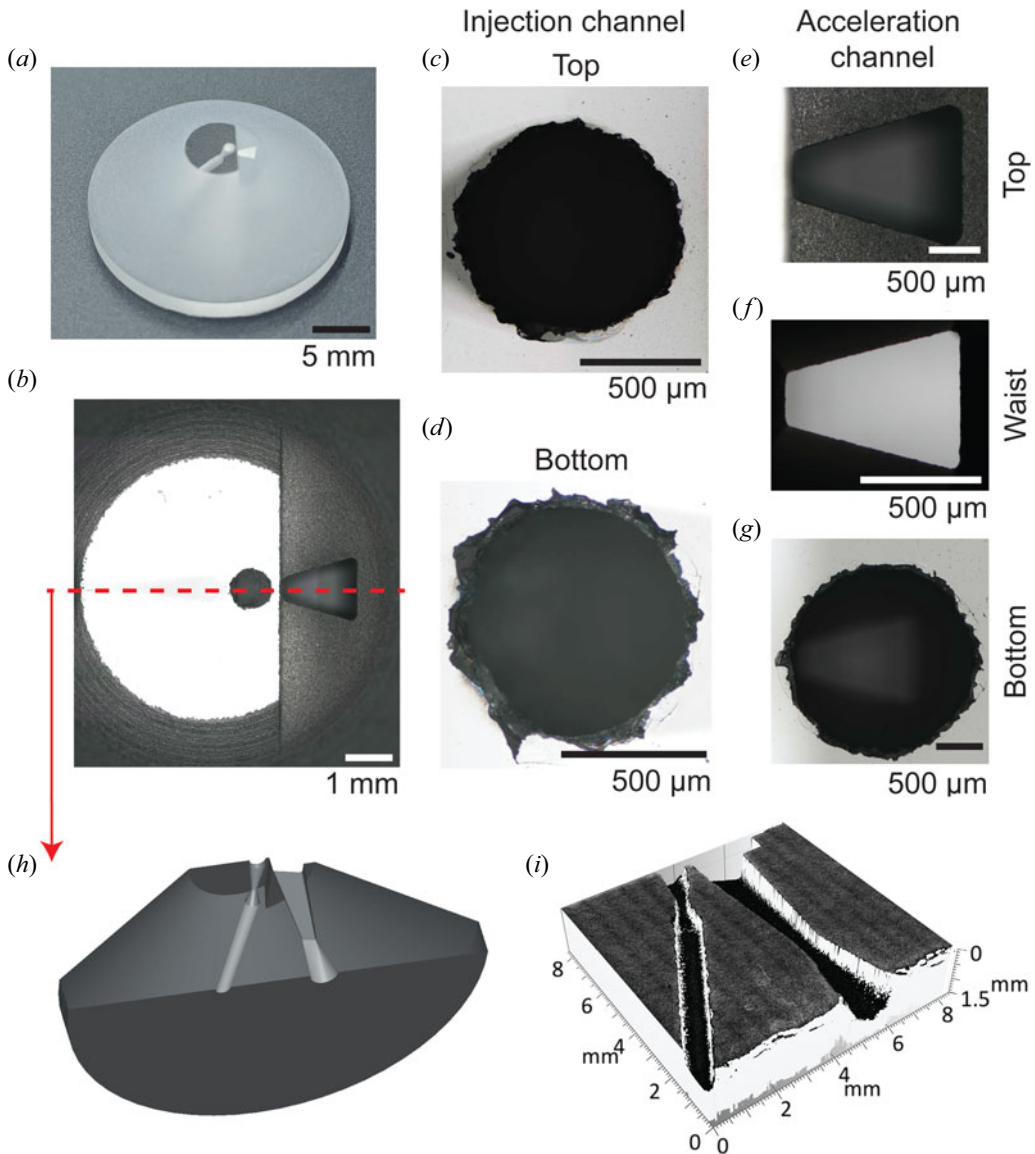
FIGURE 4. Photo of the milled nozzle (*a*). Optical microscope photographs (*b*)–(*g*). Photograph of the top surface of the nozzle (*b*). The entire image was made from a programmatically stitched sequence of photographs taken at different Z-heights. The injection channel at the top (*c*) and bottom (*d*). The acceleration nozzle at different positions is shown in (*e*)–(*g*). Section of nozzle drawing (*h*) and topography of cut nozzle channels (*i*).

this may have been that high air pressure was blown into the channels, and at the end of the milling, a thin layer of glass at the bottom surface was fractured.

A drawing of the entire section of the nozzle channels is shown in figure 4(*h*). The nozzle was cut through using the same bottom-up milling technique to view the milled channels. The topography of the cut channels can be seen in figure 4(*i*). After cutting, the surface roughness of the channels in the vertical direction (along the flow direction) was measured. The acceleration channel had an R_a of 1.6 µm and R_z of 11.3 µm. The surface

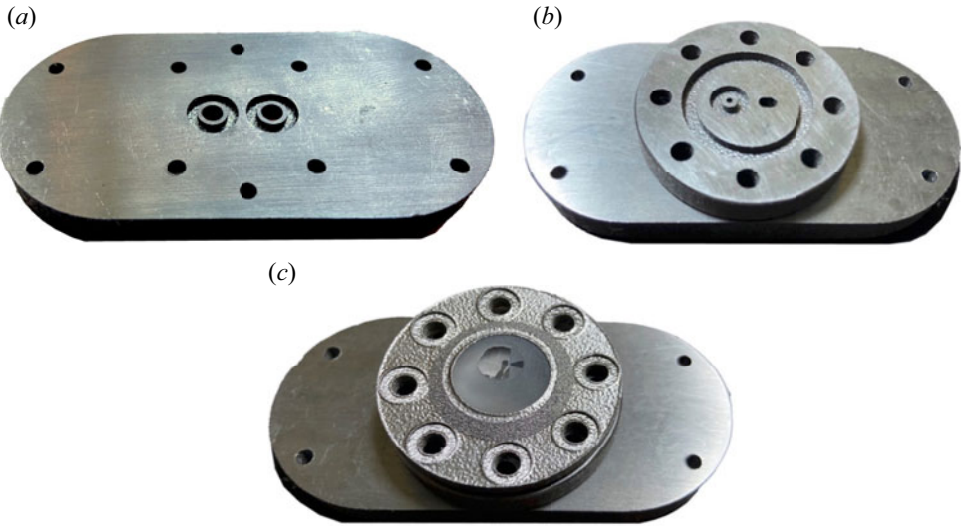(*a*)   (*b*)

(*c*)

FIGURE 5. Two-valve adapter for supplying different gases to the nozzle (*a*,*b*) and image of the assembled nozzle with two different gas supply systems (*c*).

quality of the inclined injection channel was poorer, with R_a of 4.1 µm and R_z of 21.4 µm. This was comparable to the roughness of the plane part of the nozzle with R_a of 4.1 µm and R_z of 31.7 µm.

To connect the nozzle to two different gas supply systems, using two Parker type 9 valves, two adapters and a conical mounting ring were made of stainless steel by three-dimensional laser printing (figure 5*a*,*b*). An image of the assembled nozzle with adapters is shown in figure 5(*c*).

5. Concluding remarks

In this work, a two-stage supersonic nozzle was proposed to optimise the injection and acceleration of electrons. The first stage of the nozzle is used for ionisation injection of electrons and adjustment of the position of the injected electrons into the rear part of the plasma bubble. The second stage of the nozzle is dedicated to the LWFA acceleration of electrons and ensures the maximal acceleration distance and low energy spread of the electrons. The gas density was simulated using the OpenFOAM CFD software and the designed nozzle was manufactured from a single fused silica block using a three-dimensional nanosecond rear-side processing technique.

Acknowledgements

Funding

Declaration of interest

The authors report no conflict of interest.

Data availability

The authors confirm that all of the data and codes used in this study are available from the corresponding author upon reasonable request.

REFERENCES

ANDRIANAKI, G., GRIGORIADIS, A., SKOULAKIS, A., TAZES, I., MANCELLI, D., FITILIS, I., DIMITRIOU, V., BENIS, E., PAPADOGIANNIS, N. & TATARAKIS, M. 2023 Design, manufacturing, evaluation, and performance of a 3D-printed, custom-made nozzle for laser wakefield acceleration experiments. *Rev. Sci. Instrum.* **94** (10).

BUCK, A., WENZ, J., XU, J., KHRENNIKOV, K., SCHMID, K., HEIGOLDT, M., MIKHAILOVA, J.M., GEISSLER, M., SHEN, B. & KRAUSZ, F. 2013 Shock-front injector for high-quality laser-plasma acceleration. *Phys. Rev. Lett.* **110** (18), 185006.

CAI, Y., LIU, Z. & SHI, Z. 2017 Effects of dimensional size and surface roughness on service performance for a micro Laval nozzle. *J. Micromech. Microengng* **27** (5), 055001.

CAI, Y., LIU, Z., SHI, Z., SONG, Q. & WAN, Y. 2015 Optimization of machining parameters for micro-machining nozzle based on characteristics of surface roughness. *Intl J. Adv. Manuf. Technol.* **80**, 1403–1410.

CAI, Y., LIU, Z., SHI, Z., SONG, Q. & WAN, Y. 2016 Influence of machined surface roughness on thrust performance of micro-nozzle manufactured by micro-milling. *Exp. Therm. Fluid Sci.* **77**, 295–305.

CHAULAGAIN, U., KARATODOROV, S., RACLAVSKÝ, M., LORENZ, S., LAMAČ, M., ALBRECHT, M., TOMKUS, V., DUDUTIS, J., MACKEVIČIŪTĖ, M. & GEČYS, P. 2021 Tomographic characterization of gas jets for laser-plasma acceleration with increased sensitivity. *Proceedings of SPIE 11886, International Conference on X-Ray Lasers 2020*, 118860A.

CHEN, G., XIONG, Q., MORRIS, P.J., PATERSON, E.G., SERGEEV, A. & WANG, Y. 2014 OpenFOAM for computational fluid dynamics. *Not. AMS* **61** (4), 354–363.

CHIOMENTO, B.B., ZUFFI, A.V., VIEIRA, N.D. JR., TABACOW, F.B., MALDONADO, E.P. & SAMAD, R.E. 2021 Development of dielectric de Laval nozzles for laser electron acceleration by ultrashort pulses micromachining. *2021 SBFoton International Optics and Photonics Conference (SBFoton IOPC)*, 31 May–2 June 2021, Sao Carlos, Brazil. IEEE.

DE LA OSSA, A.M., HU, Z., STREETER, M., MEHRLING, T., KONONENKO, O., SHEERAN, B. & OSTERHOFF, J. 2017 Optimizing density down-ramp injection for beam-driven plasma wakefield accelerators. *Phys. Rev. Accel. Beams* **20** (9), 091301.

DÖPP, A., GUILLAUME, E., THAURY, C., GAUTIER, J., TA PHUOC, K. & MALKA, V. 2016 3D printing of gas jet nozzles for laser-plasma accelerators. *Rev. Sci. Instrum.* **87** (7).

EKERFELT, H., HANSSON, M., GALLARDO GONZÁLEZ, I., DAVOINE, X. & LUNDH, O. 2017 A tunable electron beam source using trapping of electrons in a density down-ramp in laser wakefield acceleration. *Sci. Rep.* **7** (1), 12229.

FOERSTER, F., DÖPP, A., HABERSTROH, F., GRAFENSTEIN, K.V., CAMPBELL, D., CHANG, Y.-Y., CORDE, S., CABADAĞ, J.C., DEBUS, A. & GILLJOHANN, M. 2022 Stable and high-quality electron beams from staged laser and plasma wakefield accelerators. *Phys. Rev.* X **12** (4), 041016.

GEČYS, P., DUDUTIS, J. & RAČIUKAITIS, G. 2015 Nanosecond laser processing of soda-lime glass. *J. Laser Micro/Nanoengng* **10**, 3.

GOLOVIN, G., BANERJEE, S., CHEN, S., POWERS, N., LIU, C., YAN, W., ZHANG, J., ZHANG, P., ZHAO, B. & UMSTADTER, D. 2016 Control and optimization of a staged laser-wakefield accelerator. *Nucl. Instrum. Meth. Phys. Res. Sect.* A*: Accel. Spectrom. Detect. Assoc. Equip.* **830**, 375–380.

GONSALVES, A., NAKAMURA, K., LIN, C., PANASENKO, D., SHIRAISHI, S., SOKOLLIK, T., BENEDETTI, C., SCHROEDER, C., GEDDES, C. & VAN TILBORG, J. 2011 Tunable laser plasma accelerator based on longitudinal density tailoring. *Nat. Phys.* **7** (11), 862–866.

GUILLAUME, E., DÖPP, A., THAURY, C., PHUOC, K.T., LIFSCHITZ, A., GRITTANI, G., GODDET, J.-P., TAFZI, A., CHOU, S.-W. & VEISZ, L. 2015 Electron rephasing in a laser-wakefield accelerator. *Phys. Rev. Lett.* **115** (15), 155002.

HE, Z. 2014 Laser wakefield acceleration using few-millijoule laser pulses at kilohertz repetition-rate. PhD Thesis, University of Michigan.

KALMYKOV, S., YI, S., KHUDIK, V. & SHVETS, G. 2009 Electron self-injection and trapping into an evolving plasma bubble. *Phys. Rev. Lett.* **103** (13), 135004.

KIM, H.T., PAE, K.H., CHA, H.J., KIM, I.J., YU, T.J., SUNG, J.H., LEE, S.K., JEONG, T.M. & LEE, J. 2013 Enhancement of electron energy to the multi-GeV regime by a dual-stage laser-wakefield accelerator pumped by petawatt laser pulses. *Phys. Rev. Lett.* **111** (16), 165002.

LI, H., WANG, Y., WANG, Z. & ZHAO, Z. 2018 Fabrication of ZrB2–SiC–graphite ceramic micro-nozzle by micro-EDM segmented milling. *J. Micromech. Microengng* **28** (10), 105022.

LIU, J., XIA, C., WANG, W., LU, H., WANG, C., DENG, A., LI, W., ZHANG, H., LIANG, X. & LENG, Y. 2011 All-optical cascaded laser wakefield accelerator using ionization-induced injection. *Phys. Rev. Lett.* **107** (3), 035001.

MANGLES, S.P., GENOUD, G., BLOOM, M.S., BURZA, M., NAJMUDIN, Z., PERSSON, A., SVENSSON, K., THOMAS, A.G.R. & WAHLSTRÖM, C.-G. 2012 Self-injection threshold in self-guided laser wakefield accelerators. *Phys. Rev. Spec. Topics Accel. Beams* **15** (1), 011302.

MASSIMO, F., LIFSCHITZ, A., THAURY, C. & MALKA, V. 2017 Numerical studies of density transition injection in laser wakefield acceleration. *Plasma Phys. Control. Fusion* **59** (8), 085004.

MCGUFFEY, C., THOMAS, A., SCHUMAKER, W., MATSUOKA, T., CHVYKOV, V., DOLLAR, F., KALINTCHENKO, G., YANOVSKY, V., MAKSIMCHUK, A. & KRUSHELNICK, K. 2010 Ionization induced trapping in a laser wakefield accelerator. *Phys. Rev. Lett.* **104** (2), 025004.

OPENFOAM. 2022 Available at: https://www.openfoam.com/.

OUBRERIE, K., ANDRIYASH, I.A., LAHAYE, R., SMARTSEV, S., MALKA, V. & THAURY, C. 2022 Axiparabola: a new tool for high-intensity optics. *J. Opt.* **24** (4), 045503.

PAK, A., MARSH, K., MARTINS, S., LU, W., MORI, W. & JOSHI, C. 2010 Injection and trapping of tunnel-ionized electrons into laser-produced wakes. *Phys. Rev. Lett.* **104** (2), 025003.

POLLOCK, B., CLAYTON, C., RALPH, J., ALBERT, F., DAVIDSON, A., DIVOL, L., FILIP, C., GLENZER, S., HERPOLDT, K. & LU, W. 2011 Demonstration of a narrow energy spread, ~0.5 GeV electron beam from a two-stage laser wakefield accelerator. *Phys. Rev. Lett.* **107** (4), 045001.

PUKHOV, A. & KOSTYUKOV, I. 2008 Control of laser-wakefield acceleration by the plasma-density profile. *Phys. Rev.* E **77** (2), 025401.

ROVIGE, L., HUIJTS, J., ANDRIYASH, I., VERNIER, A., TOMKUS, V., GIRDAUSKAS, V., RACIUKAITIS, G., DUDUTIS, J., STANKEVIC, V. & GECYS, P. 2020 Demonstration of stable long-term operation of a kilohertz laser-plasma accelerator. *Phys. Rev. Accel. Beams* **23** (9), 093401.

ROVIGE, L., HUIJTS, J., VERNIER, A., ANDRIYASH, I., SYLLA, F., TOMKUS, V., GIRDAUSKAS, V., RACIUKAITIS, G., DUDUTIS, J. & STANKEVIC, V. 2021 Symmetric and asymmetric shocked gas jets for laser-plasma experiments. *Rev. Sci. Instrum.* **92** (8).

SAMANT, S.A., UPADHYAY, A.K. & KRISHNAGOPAL, S. 2014 High brightness electron beams from density transition laser wakefield acceleration for short-wavelength free-electron lasers. *Plasma Phys. Control. Fusion* **56** (9), 095003.

SCHMID, K., BUCK, A., SEARS, C.M., MIKHAILOVA, J.M., TAUTZ, R., HERRMANN, D., GEISSLER, M., KRAUSZ, F. & VEISZ, L. 2010 Density-transition based electron injector for laser driven wakefield accelerators. *Phys. Rev. Spec. Topics Accel. Beams* **13** (9), 091301.

SMARTSEV, S., CAIZERGUES, C., OUBRERIE, K., GAUTIER, J., GODDET, J.-P., TAFZI, A., PHUOC, K.T., MALKA, V. & THAURY, C. 2019 Axiparabola: a long-focal-depth, high-resolution mirror for broadband high-intensity lasers. *Opt. Lett.* **44** (14), 3414–3417.

SPRANGLE, P., HAFIZI, B., PENANO, J., HUBBARD, R., TING, A., MOORE, C., GORDON, D., ZIGLER, A., KAGANOVICH, D. & ANTONSEN, T. JR. 2001 Wakefield generation and GeV acceleration in tapered plasma channels. *Phys. Rev.* E **63** (5), 056405.

STEINKE, S., VAN TILBORG, J., BENEDETTI, C., GEDDES, C., SCHROEDER, C., DANIELS, J., SWANSON, K., GONSALVES, A., NAKAMURA, K. & MATLIS, N. 2016 Multistage coupling of independent laser-plasma accelerators. *Nature* **530** (7589), 190–193.

SUK, H., BAROV, N., ROSENZWEIG, J.B. & ESAREY, E. 2001 Plasma electron trapping and acceleration in a plasma wake field using a density transition. *Phys. Rev. Lett.* **86** (6), 1011.

TAJIMA, T. & MALKA, V. 2020 Laser plasma accelerators. *Plasma Phys. Control. Fusion* **62** (3), 034004.

TAKAHASHI, S., HORIUCHI, K., MORI, S., TATSUKOSHI, K., ONO, M., MIKAYAMA, M., IMAJO, N. & MOBLEY, T. 2013 Development of through glass via technology for 3D packaging. In *EMPC 2013 - European Microelectronics and Packaging Conference – The Winding Roads of Electronics Packaging,* 9–12 September 2013, Grenoble, France. IEEE, pp. 1–5.

TOMKUS, V., GIRDAUSKAS, V., DUDUTIS, J., GEČYS, P., STANKEVIČ, V. & RAČIUKAITIS, G. 2018 High-density gas capillary nozzles manufactured by hybrid 3D laser machining technique from fused silica. *Opt. Express* **26** (21), 27965–27977.

TOMKUS, V., GIRDAUSKAS, V., DUDUTIS, J., GEČYS, P., STANKEVIČ, V. & RAČIUKAITIS, G. 2019 Impact of the wall roughness on the quality of micrometric nozzles manufactured from fused silica by different laser processing techniques. *Appl. Surf. Sci.* **483**, 205–211.

TOMKUS, V., GIRDAUSKAS, V., DUDUTIS, J., GEČYS, P., STANKEVIČ, V., RAČIUKAITIS, G., GONZÁLEZ, I.G., GUÉNOT, D., SVENSSON, J.B. & PERSSON, A. 2020 Laser wakefield accelerated electron beams and betatron radiation from multijet gas targets. *Sci. Rep.* **10** (1), 1–17.

TÓTH, S., NAGYMIHÁLY, R.S., SERES, I., LEHOTAI, L., CSONTOS, J., TÓTH, L.T., GEETHA, P.P., SOMOSKŐI, T., KAJLA, B. & ABT, D. 2023 Single thin-plate compression of multi-TW laser pulses to 3.9 fs. *Opt. Lett.* **48** (1), 57–60.

VARGAS, M., SCHUMAKER, W., HE, Z.-H., ZHAO, Z., BEHM, K., CHVYKOV, V., HOU, B., KRUSHELNICK, K., MAKSIMCHUK, A. & YANOVSKY, V. 2014 Improvements to laser wakefield accelerated electron beam stability, divergence, and energy spread using three-dimensional printed two-stage gas cell targets. *Appl. Phys. Lett.* **104** (17).

VIEIRA, J., FIÚZA, F., SILVA, L., TZOUFRAS, M. & MORI, W. 2010 Onset of self-steepening of intense laser pulses in plasmas. *New J. Phys.* **12** (4), 045025.

WANG, W., FENG, K., KE, L., YU, C., XU, Y., QI, R., CHEN, Y., QIN, Z., ZHANG, Z. & FANG, M. 2021 Free-electron lasing at 27 nanometres based on a laser wakefield accelerator. *Nature* **595** (7868), 516–520.

WANG, W., LI, W., LIU, J., WANG, C., CHEN, Q., ZHANG, Z., QI, R., LENG, Y., LIANG, X. & LIU, Y. 2013 Control of seeding phase for a cascaded laser wakefield accelerator with gradient injection. *Appl. Phys. Lett.* **103** (24).

WAN, Y., SEEMANN, O., TATA, S., ANDRIYASH, I.A., SMARTSEV, S., KROUPP, E. & MALKA, V. 2022 Direct observation of relativistic broken plasma waves. *Nat. Phys.* **18** (10), 1186–1190.

XU, X., LI, F., AN, W., DALICHAOUCH, T., YU, P., LU, W., JOSHI, C. & MORI, W. 2017 High quality electron bunch generation using a longitudinal density-tailored plasma-based accelerator in the three-dimensional blowout regime. *Phys. Rev. Accel. Beams* **20** (11), 111303.

ZHANG, G.-B., CHEN, M., ZOU, D.-B., ZHU, X.-Z., LI, B.-Y., YANG, X.-H., LIU, F., YU, T.-P., MA, Y.-Y. & SHENG, Z.-M. 2022 Carrier-envelope-phase-controlled acceleration of multicolored attosecond electron bunches in a millijoule-laser-driven wakefield. *Phys. Rev. Appl.* **17** (2), 024051.

ZUFFI, A.V., TABACOW, F.B., VIEIRA, N.D. & SAMAD, R.E. 2022 Ultrafast laser micromachining of submillimetric de Laval nozzles in alumina for laser electron acceleration. *2022 SBFoton International Optics and Photonics Conference (SBFoton IOPC),* 13–15 October 2022, Recife, Brazil. IEEE.